2019 SECED Conference
Earthquake risk and engineering towards a resilient world
9-10 September 2019, Greenwich, London

COLLAPSE AND DEMOLITION AFTERSHOCK ASSESSMENT OF POST-MAINSHOCK STEEL FRAMED BUILDINGS

Jorge RUIZ-GARCÍA[1]

Abstract: *This paper describes and evaluates a methodology to compute the collapse and demolition capacity of buildings under aftershocks taking explicitly into account residual drift demands after the mainshock (i.e., post-mainshock residual drifts, $RIDR_o$). The methodology also allows computing measure of the residual capacity of buildings to sustain aftershocks. The methodology is applied to a testbed four-story steel moment resisting building designed with modern seismic design provisions when subjected to a set of near-fault mainshock-aftershock seismic sequences that induce five levels of $RIDR_o$. Once the post-mainshock residual drift is induced to the building model, a post-mainshok Incremental Dynamic analysis is performed under each aftershock to obtain its collapse capacity and its capacity associated to demolition (i.e., the capacity to reach or exceed a 2% residual drift). The influence of additional sources of stiffness and strength (i.e., interior gravity frames and slab contribution) is examined in this study. Results show that the collapse potential under aftershocks strongly depends on the modelling approach (i.e., the aftershock collapse potential is modified when additional sources of lateral stiffness and strength are included in the analytical model). Furthermore, it is demonstrated that the aftershock capacity associated to demolition (i.e., the aftershock collapse capacity associated to a residual inter-storey drift that lead to an imminent demolition) is lower than that of the aftershock collapse capacity, which mean that this parameter should be a better measure of the building residual capacity against aftershocks.*

Introduction

Nowadays, the aim of a modern seismic assessment method for buildings is to quantify their seismic resilience (i.e., the capacity to restore its functionality in an adequate period of time after experiencing an extreme seismic event), which should include the effects of strong aftershocks. In this context, the quantification of the post-mainshock residual capacity of the building to sustain aftershocks should be a key parameter. For instance, Polese et al. (2012) defined a residual capacity index as the minimum spectral acceleration (at the equivalent period of an equivalent single-degree-of-freedom system with an envelope associated to a given damage state obtained from pushover analysis of the building under consideration) corresponding to building collapse under a set of earthquake ground motions. However, it should be noted that in-situ permanent (residual) displacements are a measurable seismic demand after the mainshock, which can be determined using, for example, robotic theodolites (e.g., Psimoulis and Stiros 2007) during post-mainshock field reconnaissance. Therefore, it is believed that an alternative approach for structural seismic assessment under aftershocks should be based in the explicit consideration of post-mainshock residual drifts that a structure would experience.

The objective of the research reported in this paper is to introduce a methodology for the seismic assessment of the collapse and demolition capacity of post-mainshock steel framed buildings under aftershocks. Under this approach, measures of residual capacity are also introduced in this paper.

Methodology

A methodology for assessing the seismic performance against aftershocks is presented in this study, which takes explicitly into account the amplitude of lateral residual drift demands after the mainshock seismic event. Particularly, the methodology can be applied for computing the collapse potential against aftershocks, the demolition capacity, and the residual post-mainshock capacity. The key steps of the methodology are described next:

[1] Professor, Universidad Michoacana de San Nicolás de Hidalgo, Morelia, México, jruizgar@stanfordalumni.org

A) To develop an appropriate analytical model of a case-study building, in its undamaged condition.
B) To select a set of mainshock-aftershock seismic sequences representative of the seismic hazard of the site of interest.
C) To select different levels of residual drift (e.g. maximum residual inter-story drift ratio or roof residual drift ratio) after the mainshock earthquake excitation named as target post-mainshock residual drifts.
D) To scale, in amplitude, each as-recorded mainshock earthquake ground motion in such manner that the building model reaches the selected target post-mainshock residual drift under the scaled mainshock ground motion.
E) To carry out incremental dynamic analysis (IDA) of the leaned building (i.e., in its post-mainshock condition selected in the previous step) under the corresponding aftershock ground motion record up to collapse. Collapse can be defined when the building exhibits dynamic instability due to large lateral drift demands.

In this study, the spectral acceleration corresponding to the fundamental period of the building, $S_a(T_1)$, was selected as ground motion intensity measure of both the mainshock and aftershock earthquake ground motions. Therefore, the seismic intensity associated to collapse under the aftershock is designated as $S_{a,A}$ (i.e., the aftershock collapse capacity), while the mainshock collapse capacity can be computed from IDA of the undamaged case-study building, which is named $S_{a,M}$. After computing both collapse capacities, the residual capacity index to sustain aftershocks can be computed as follows:

$$\kappa = \frac{S_{a,A}}{S_{a,M}} \tag{1}$$

It should be mentioned that post-earthquake field evidence noted that excessive lateral residual drifts could lead the building under consideration to demolition (Iwata et al., 2006). Therefore, it is interest to evaluate the aftershock capacity associated to demolition, $S_{a,D}$ (i.e., the seismic intensity associated to a lateral residual drift demand that drive the building to its demolition, for instance 2%).

Case-study building considered in this study

Description

For illustrating the proposed aftershock assessment procedure, a four-story steel building was selected in this investigation. The building under consideration was specifically designed to investigate the collapse prediction of modern steel structures located in sites of high seismicity (Lignos and Krawinkler, 2011), and served as a prototype for developing one-eight scale models tested in a shake-table facility. Figure 1 shows the plan view and elevation of the prototype building. The prototype was designed following the IBC–2003 and AISC–341-05 standards in the U.S. As usual in American design practice, the building includes perimeter moment-resisting frames along with interior gravity frames. Particularly, as recommended for modern steel construction, the beams where designed with reduced beam sections.

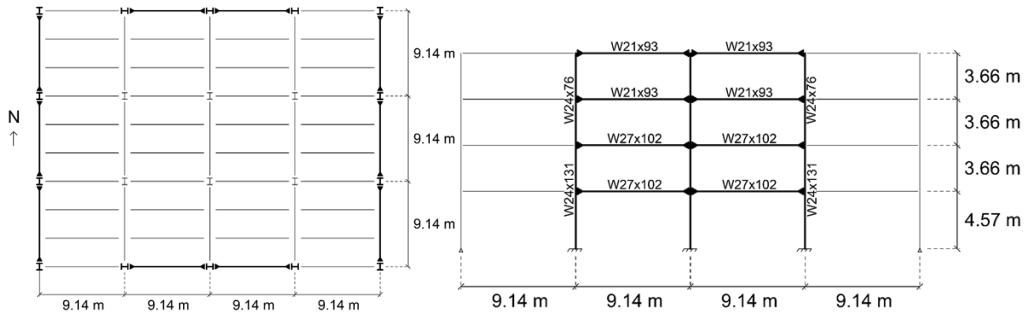

Figure 1. Case-study steel framed-building considered in this study: a) Plan view, b) East-West elevation.

Modelling

The testbed building was modelled using the computational platform OpenSees (2014). Only half of the building was modelled due to its symmetry in the building's plan. Two analytical two-dimensional models were developed for this investigation: a) model M1, that only includes the exterior East-West moment-resisting frame, and b) model M2, that incorporates several additional sources of lateral stiffness and strength. It should be noted that model M1 includes an additional fictitious column, which is a common modelling strategy in the U.S. In this modelling approach, the fictitious column carries the vertical (gravity) loading from the rest of building (i.e., vertical loading carried by the interior gravity columns) and it is attached to the exterior frame model through rigid frame elements that experience the same lateral deformation at each floor. However, the fictitious column does not provide the additional lateral stiffness from the interior gravity columns. In contrast, model M2 includes explicitly one interior gravity frame in addition to the exterior frame.

In both models, beams and columns were modelled as two-dimensional, prismatic beam elements composed of an elastic beam element with rotational springs at the ends that concentrates the element's nonlinear moment-rotation hysteretic behaviour (Zareian and Medina, 2009). The hysteretic behaviour in the rotational springs accounts for structural cyclic degradation (i.e., strength and stiffness degradation) using the modified Ibarra-Medina-Krawinkler (MIK) model introduced in (Lignos and Krawinkler, 2011a) and implemented in the *OpenSees* platform (2014). The parameters of the backbone curve in the MIK model for beams were obtained from those proposed in (Lignos and Krawinkler, 2011a). In addition, panel zone flexibility was taken into account in each model following the modelling technique proposed in (ATC, 2010). It should be noted that the slab contribution was not taken into account in the beam's stiffness and strength for model M1, which is consistent with the modelling assumptions followed by Lignos and Krawinkler (2011b). However, the contribution of the slab was explicitly included in model M2 by using a larger beam's moment of inertia and asymmetric moment-rotation hysteretic relationship (i.e., with moment capacity in the positive bending direction 10% greater than that in the negative bending direction). In addition to identical modelling strategies in the exterior moment-resisting frame, model M2 included two additional gravity-frame bays and one interior gravity frame. The interior beams were also modelled taking into account their moment capacity. Before performing nonlinear dynamic analysis, conventional modal analysis and nonlinear static (pushover) analysis were carried out to obtain the dynamic and mechanical properties of both building models. Figure 2 shows a comparison of the capacity curve corresponding to building models M1 and M2, while Table 1 reports relevant dynamic and mechanical feature. From the figure, it can clearly be seen that the additional sources of stiffness and strength have significant influence in the capacity curve.

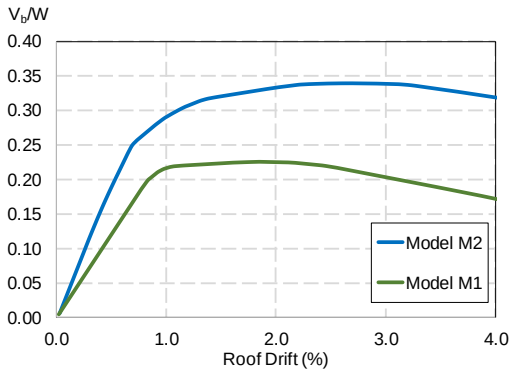

Figure 2. Comparison of capacity curves for building models M1 and M2.

Building model	T_1 (s)	C_y	θy (%)	$\Gamma_1 \Phi_{1,roof}$
M1	1.28	0.26	0.92	1.29
M2	1.06	0.36	0.88	1.28

Table 1. Dynamic and mechanical properties of the building models (T_1 is the first-mode period of vibration, C_y is the yield strength coefficient, θy is the roof drift at yielding, and $\Gamma_1 \phi_{1,roof}$ is the normalized modal participation factor).

Next, nonlinear dynamic time-history analyses were carried out using Newmark constant average acceleration method with time step equal to 0.001s to enhance convergence. Rayleigh damping equal to 3% of critical was assigned to the first and second modes. During the analysis, local P-delta effects were included (i.e., large displacement analysis).

Aftershock collapse assessment under individual seismic sequences

Set of mainshock-aftershock seismic sequences

Although the outlined methodology is general, a set of 13 near fault mainshock-aftershock ground motion pairs gathered in accelerographic stations during the 1994 Northridge earthquakes was selected to illustrate the methodology. A detailed list of the ground motion features of the seismic sequences considered in this study can be found in Ruiz-García and Negrete-Manriquez (2011).

Target maximum residual drift demands

The proposed methodology requires defying relevant post-mainshock residual drifts (e.g. maximum residual inter-storey drift or the roof residual drift). For example, a field survey of reinforced concrete buildings built in Japan highlighted that a residual inter-storey drift of about 0.5% is perceptible for building occupants and a residual inter-storey drift of about 1.0% could cause human discomfort (McCormick et al., 2008). On the other hand, Iwata et al. (2006) reported that the cost of repair leaned steel buildings after the 1995 Kobe earthquake linearly increased as the maximum and roof residual drift increased. Based on their observations, the authors suggested that steel buildings should be limited to maximum residual interstory and roof residual drift limits of about 1.4% and 0.9%, respectively, to satisfy a reparability limit state that meet both technical and economic constraints. Similarly, FEMA P-58 (2012) recommendations describe that a maximum residual inter-storey drift of 2% in a building implies that there is a certainty that it will not be repaired. Therefore, based on the aforementioned recommendations, five target $RIDR_o$ ($RIDR_o$ =0.1%, 0.5%, 1.0%, 1.4%, and 2.0%) values were chosen in this study. For this purpose, each mainshock earthquake ground motion was scaled, in amplitude, so that each undamaged case-study building reaches $RIDR_o$ after performing nonlinear dynamic analysis.

Response of building models

At a first stage, IDA is carried out until the undamaged building model reaches its dynamic collapse capacity in order to compute $S_{a,M}$. For illustration purposes, Figure 3 shows the evolution of maximum, IDR_{max}, and residual, $RIDR_{max}$, inter-storey drift of both models as the intensity of the mainshock ground motion intensity grows up to collapse (noted with a black circle) using the earthquake ground motion recoded at Sylmar Converter station (comp. 288). IDR_{max} is presented in absolute value, while $RIDR_{max}$ is shown in relative value with respect to the initial position. As it might be anticipated, the model M2 has greater collapse capacity than model M1 since it includes additional sources of overstrength. Interestingly, model M1 develops a re-centering behaviour (i.e., it moves back to its initial position after experiencing residual drifts in one direction), unlike model M2. The effect of re-centering behaviour in the aftershock collapse capacity is discussed later.

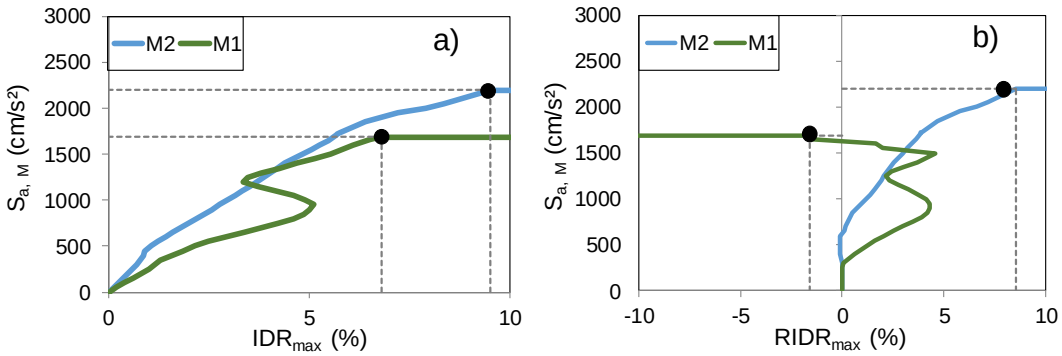

Figure 3. IDA curves to obtain the mainshock collapse capacity of the models M1 and M2 under Sylmar (comp. 288) record: a) IDR_{max}, and b) $RIDR_{max}$.

At a second stage, the mainshock acceleration time-history recorded at Sylmar (comp. 288) station was scaled, in amplitude, up to each building model reach six levels of $RIDR_o$. After reaching each target residual drift, IDA was applied to each building model under the Sylmar aftershock earthquake ground motion to compute its $S_{a,A}$. For illustration purposes, Figure 4 shows the aftershock IDA curves for IDR_{max} and $RIDR_{max}$ corresponding to each target $RIDR_o$ for model M2. As it may be expected, the aftershock collapse capacity depends on the level of $RIDR_o$. For example, $S_{a,A}$ for a $RIDR_o$ equal to 0.1% reduces from about 1150 cm/s^2 (1.17g) to 1070 cm/s^2 (1.07g) for a $RIDR_o$ equal to 2.0%. Additionally, it can be observed that $S_{a,A}$ decreases with respect to the $S_{a,M}$ regardless of the target $RIDR_o$. For example, the aftershock collapse capacity reduces from about 2200 cm/s^2 (2.24g) to 1070 cm/s^2 (1.07g) for target $RIDR_o$ equal to 1.4%, which means a residual capacity index around 0.48 (i.e., reduction of 52% in its original collapse capacity).

If a $RIDR_{max}$ equal to 2% is related to imminent demolition of the building, the demolition capacity, $S_{a,D}$, can be computed from Figure 4b for each level of $RIDR_o$. From the figure, it can clearly be seen that $S_{a,D}$ is smaller than that associated to $S_{a,A}$ for each level of $RIDR_o$. This main observation implies that the aftershock capacity of buildings that experience a post-mainshock inter-storey residual drift should be measured in terms of the remaining capacity to limit the building to sustain a threshold residual inter-storey drift related to demolition in the event of a strong aftershock rather than the capacity to collapse under the aftershock.

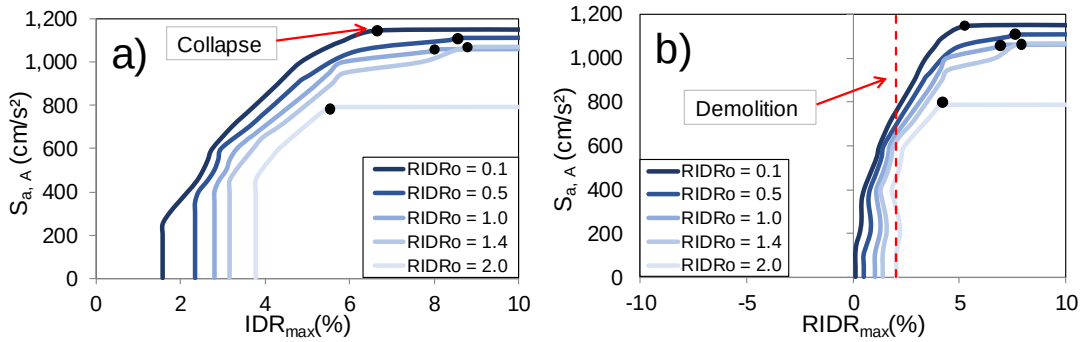

Figure 4. Post-mainshock IDA curves to obtain the aftershock collapse capacity of the M2 building model under the aftershock recorded at Sylmar station: a) IDR_{max}, and b) $RIDR_{max}$.

Next, Figure 5 shows a comparison of post-mainshock IDA curves corresponding to models M1 and M2 for a $RIDR_o$ equal to 1.0%. The $S_{a,A}$ and $S_{a,D}$ are indicated in the figure with black and orange circles, respectively. It can be seen that the $S_{a,A}$ and $S_{a,D}$ strongly depend on the modelling approach since the model M2 have greater collapse and demolition capacities than model M1 (e.g., $S_{a,D}$ is approximately equal to 200 and 650 cm/s^2 for models M1 and M2, respectively). Nonetheless, $S_{a,D}$ is about 60% of $S_{a,A}$ for model M2, which highlight the importance of computing the demolition capacity. Similar observations were found from other levels of $RIDR_o$.

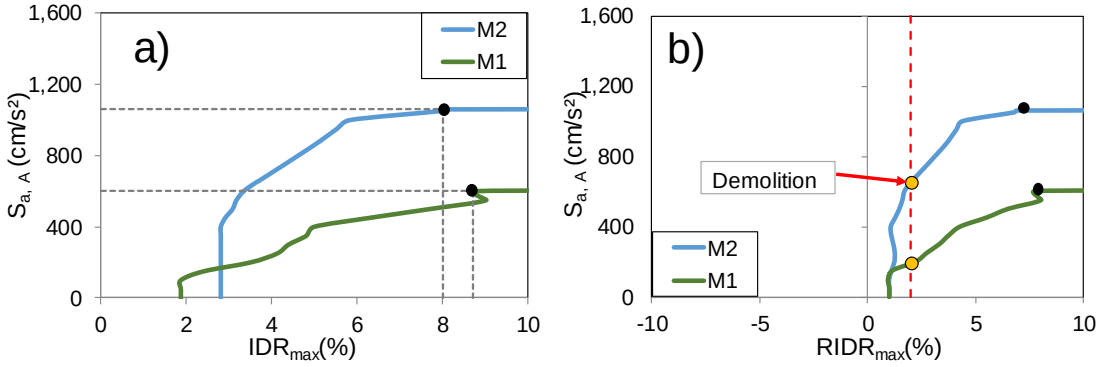

Figure 5. Comparison of post-mainshock IDA curves corresponding to models M1 and M2 under the aftershock recorded at Sylmar station: a) IDR_{max}, and b) $RIDR_{max}$.

In terms of estimating the residual capacity of the models, it was found that the residual capacity index is very similar for both building models under this selected earthquake ground motion, as it can be seen in Figure 6. From the figure, it can also be observed that κ is smaller than one (i.e., the building model has smaller collapse capacity to sustain the aftershock than that under the mainshock) and slightly decreases as the $RIDR_o$ increases.

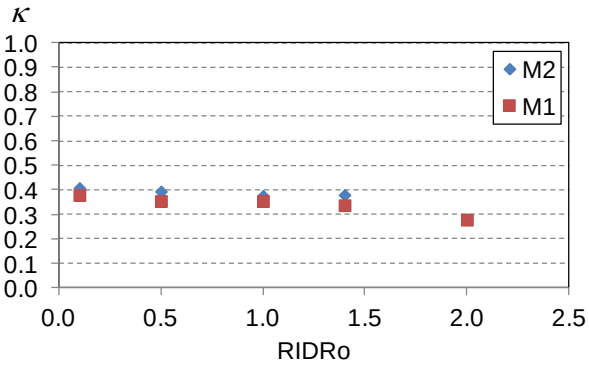

Figure 6. Variation of residual capacity index with respect to $RIDR_o$ for models M1 and M2.

However, this trend of κ was not always observed under other seismic sequences. For instance, Figure 7a illustrates the mainshock and post-mainshock IDA curves corresponding to model M2 when subjected to the earthquake ground motions recorded at Jensen Filter Plant Generator (comp. 022) station. It can be observed that $S_{a,M}$ is lower than $S_{a,A}$ regardless of the level of $RIDR_o$. For this case, the residual capacity index becomes greater than one, which means that κ might not be meaningful for measuring the collapse potential against aftershocks. Since the building model has been already carried out to a post-mainshock leaned condition, it would be more meaningful to compare its aftershock collapse capacity for different levels of $RIDR_o$ against its collapse capacity computed from the aftershock earthquake ground motion when $RIDR_o$=0% (i.e., it is assumed that the building model did not experience any post-mainshock residual drift and its original capacity remains intact) as a modified measure of its residual capacity. Therefore, Figure 7b shows the post-mainshock IDA curves including the IDA curve obtained for the intact model M2 subjected to the aftershock earthquake ground motion. Now, it can be seen that the aftershock collapse capacity for the intact case is greater than those computed for different levels of $RIDR_o$. This observation suggests redefining the residual capacity index given in Equation 1 as follows:

$$\kappa^* = \frac{S_{a,A}}{S_{a,A^*}} \tag{2}$$

where S_{a,A^*} is the aftershock collapse capacity obtained from the intact (i.e, undamaged building after the mainshock).

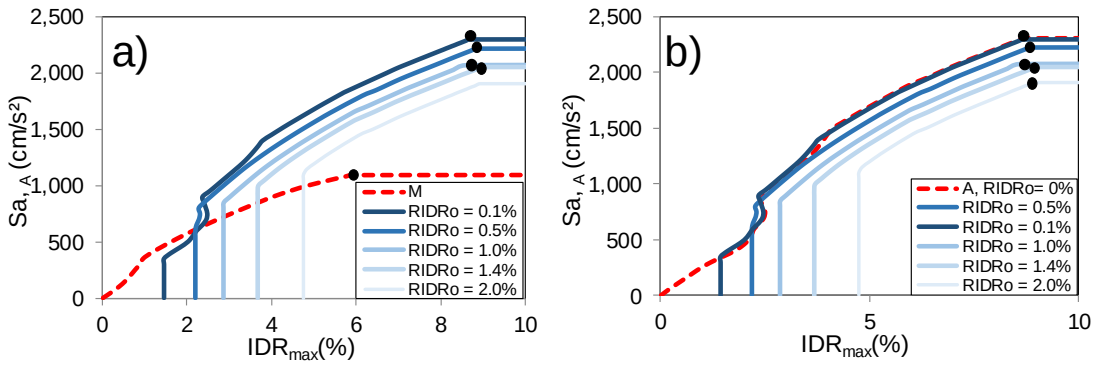

Figure 7. a) comparison of mainshock IDA and post-mainshock IDA curves; b) comparison of post-mainshock IDA curves with $RIDR_o$=0 and post-mainshock.

Re-centring behaviour under aftershocks

While developing post-mainshock IDAs under the set of aftershocks, it was noted that the case-study buildings experienced a re-centering mechanism under some aftershocks. That is, the amplitude of initial post-mainshock residual drifts tend to be smaller as the aftershock intensity grows, and the building model exhibits residual drifts in the opposite direction at high aftershock intensity levels. To illustrate this behaviour, Figure 8 shows the third-story time-story drift mainshock-aftershock response of model M2 under the sequence gathered at Tarzana station (comp. 360), corresponding to $RIDR_o$ equal to 0.1% and 2.0%. It can be seen that the aftershock earthquake ground motion, scaled to reach a $Sa,_A$ equal to 1000 cm/s^2, tends to move the building model to the opposite direction of the original post-mainshock residual drifts. However, the building model moves back to its straight position when it has already experience a post-mainshock residual drift of 2%, while the building model increases its 0.1% post-mainshock residual drift in the opposite direction. As a result of this re-centring behaviour, the aftershock collapse capacity for low $RIDR_o$ becomes smaller than that for high $RIDR_o$ as shown in Figure 9.

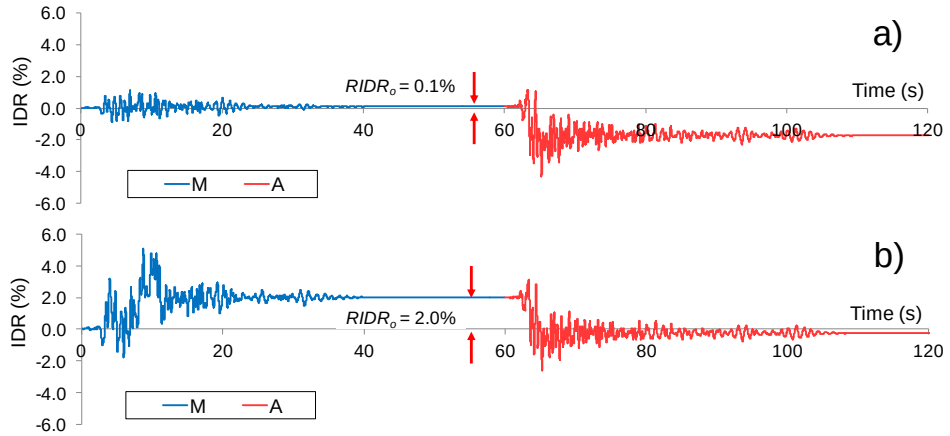

Figure 8. Re-centring behaviour observed in third-story drift time-history for two levels of $RIDR_o$: a) 0.1%, and b) 2.0%.

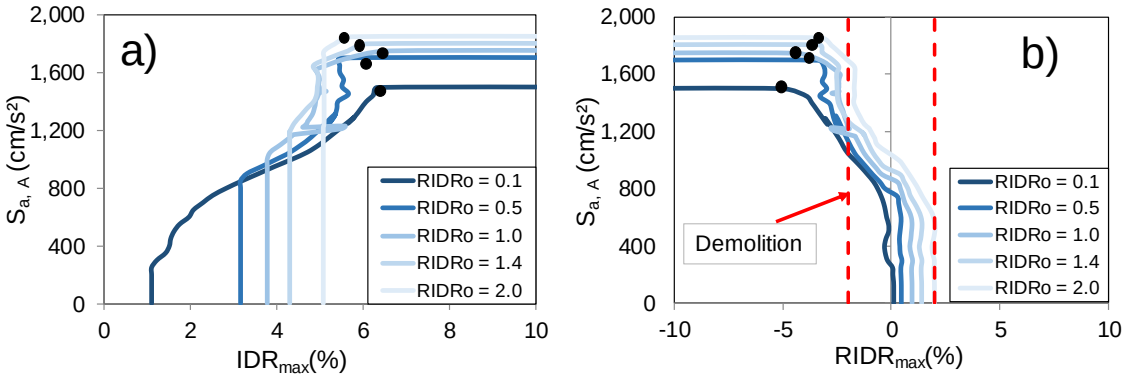

Figure 9. Post-mainshock IDA curves to obtain the aftershock collapse capacity of model M2 under the aftershock recorded at Sylmar station: a) IDR_{max}, and b) $RIDR_{max}$.

Aftershock assessment under sets of seismic sequences

Following the procedure outlined and illustrated in the previous Sections, a statistical study was conducted to evaluate $S_{a,A}$ and, particularly, the residual capacity to sustain aftershocks of models M1 and M2 under the set of mainshock-aftershock pairs. In addition, $S_{a,D}$, is also computed for each mainshock-aftershock pair and statistically examined.

Figure 10 shows the evolution of median κ with changes in the $RIDR_o$ for both M1 and M2 building models taking into account both positive (i.e., as-recorded acceleration time-history) and negative

(i.e., opposite direction of the as-recorded acceleration time-history) polarity of the aftershocks. As illustrated in Figure 10a, it can be seen that the median κ of model M1 remains stable as the $RIDR_o$ increases (e.g., from 0.51 for $RIDR_o$ equal to 0.1% to 0.63 for $RIDR_o$ equal to 2.0%). Residual capacity indices greater than one were computed in cases when the building models developed *re-centring* behavior as discussed in the previous section. As shown in Figure 10b, similar stable evolution can be observed for model M2, but its residual collapse capacity is greater than that of model M1 (e.g., from 0.92 for $RIDR_o$ equal to 0.1% to 0.88 for $RIDR_o$ equal to 2.0%). Since the model M1 experienced more cases of *re-centering* behavior, the coefficient of variation is larger than that obtained from model M2.

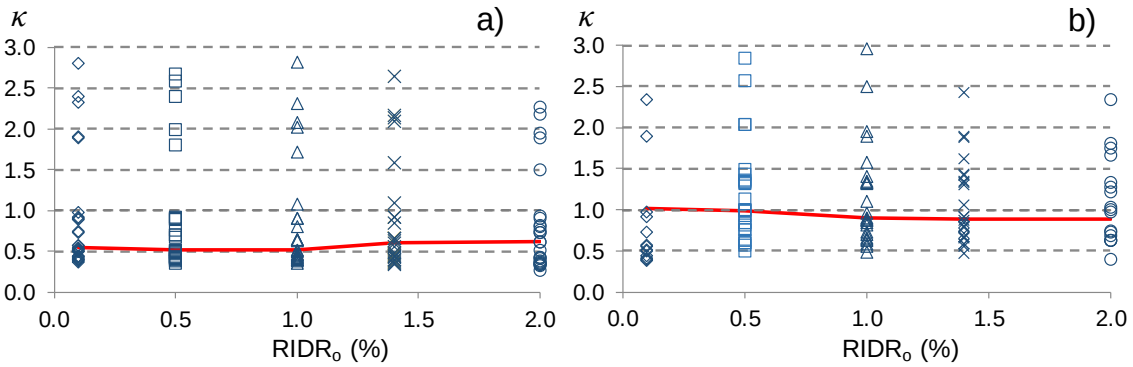

Figure 10. Residual capacity index computed from the mainshock-aftershock pairs for both models considered in this study: a) model M1; b) model M2.

The modified residual capacity index κ^* was also computed as part of this investigation. Figure 11 shows the evolution of κ^* as $RIDR_o$ increases for both building models. It can also be seen that κ^* decreases as $RIDR_o$ increases for both building models. For example, κ^* reduces from almost one for $RIDR_o$ equal to 0.1% to 0.93 and 0.78 for $RIDR_o$ equal to 1.4% and 2.0%, respectively, for building model M1. Similarly, κ^* reduces from almost one for $RIDR_o$ equal to 0.1% to 0.91 for $RIDR_o$ equal to 1.4% for building model M1. The building model M1 reaches slightly smaller values of κ^* than building model M2 since the latter model experienced more cases of re-centring behaviour, which occurred when κ^* is larger than one. For resilience-based assessment, the residual capacity of the buildings can be considered as 100% for post-mainshock residual drifts of about 0.1 and 0.5%, while decreases up to 92% and 89% for models M1 and M2, respectively, when $RIDR_o$ is equal to 1.4%. Potential readers of the paper might have expected smaller residual capacity; however, the implicit phenomenon of re-centring behaviour might help the building to keep a larger residual capacity. Finally, it should be noted that different median values of κ^* can be obtained when considering a different set of *mainshock-aftershock pairs.*

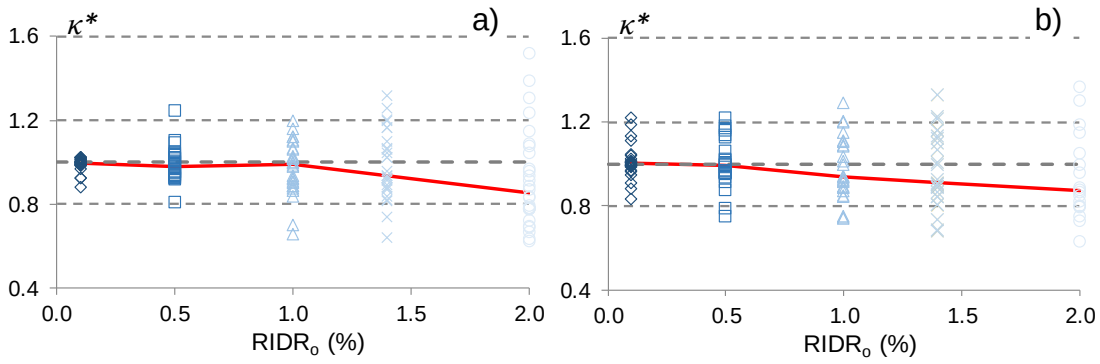

Figure 11. Modified residual capacity index computed from the set of mainshock-aftershock pairs for both models considered in this study: a) model M1; b) model M2.

As previously discussed, the aftershock capacity associated to demolition, $S_{a,D}$, is also an important parameter to evaluate for the aftershock seismic assessment. Figure 12 shows a comparison of the $S_{a,A}$ and the $S_{a,D}$ obtained from the M2 model for each individual aftershock (in bars), while the median and coefficient of variation of $S_{a,A}$ and the $S_{a,D}$ is also shown above the horizontal blue and orange dashed lines. It can clearly be observed that for some aftershocks $S_{a,D}$ is smaller, and for some cases significantly smaller, than the $S_{a,A}$. For instance, median $S_{a,D}$ is about 62% of median $S_{a,A}$ for $RIDR_o$ equal to 0.5%. Unlike median $S_{a,A}$, median $S_{a,D}$ seems to decrease in a linear fashion as $RIDR_o$ increases. Therefore, it is highlighted that the aftershock capacity associated to demolition is a key parameter to be quantified for the seismic assessment of existing structures subjected to strong aftershock, as well as for value the seismic resilience of buildings.

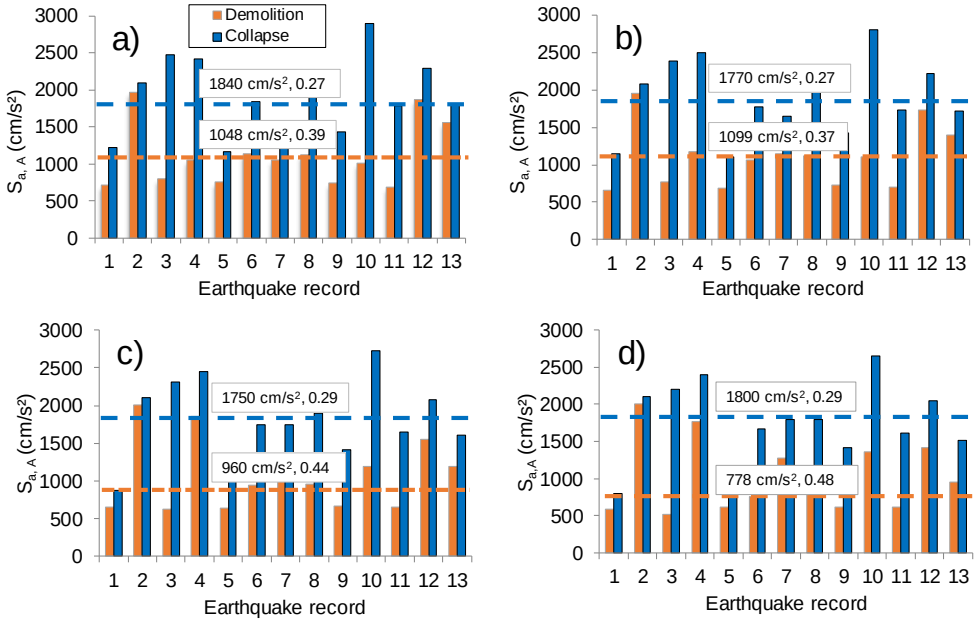

Figure 12. Comparison of $S_{a,A}$ and $S_{a,D}$ corresponding to different $RIDR_o$ for model M2: a) 0.1%; b) 0.5%, c) 1.0%, d) 1.4%.

Conclusions

This paper proposed a methodology for the seismic assessment of the collapse, $S_{a,A}$, and demolition, $S_{a,D}$, capacity of steel framed buildings under aftershocks taking explicitly into account post-mainshock residual drifts, $RIDR_o$. Applying this methodology, two measures of residual capacity can be computed. To illustrate the methodology, two analytical models of a testbed 4-storey steel frame and a set of 13 mainshock-aftershock earthquake ground motion pairs were employed in this study. Results of this investigation showed that under some mainshock-aftershocks pairs, the aftershock collapse capacity decreases as $RIDR_o$ increases. However, it was noted that both building models could experience a re-centring behaviour, which lead to an increment in the aftershock collapse capacity as $RIDR_o$ increases. Furthermore, under some mainshock-aftershock pairs, the aftershock collapse capacity was greater than the mainshock collapse capacity. Median values of κ indicate that the modelling approach has significant impact in its trend. Slightly smaller values are found when additional source of stiffness and strength (i.e., interior gravity frames, slab participation) are included in the building model. The median values of κ^* (defined as the ratio of the aftershock collapse capacity for a given level of $RIDR_o$ with respect to the aftershock collapse capacity computed from $RIDR_o$=0%) also decreases as $RIDR_o$, but the trend depended on the modelling approach. Particularly, it was highlighted that the aftershock capacity associated to demolition (i.e., associated to a 2% residual inter-storey drift) is lower than that of the aftershock collapse capacity. This capacity decreases as the level of post-mainshock residual drift increases. Since a building has to be demolished when it reaches a threshold residual inter-storey drift (e.g., 2%), the aftershock capacity associated to demolition seems a better parameter to measure the residual capacity of buildings subjected to aftershocks.

Acknowledgements

The first author would like to thank Mr. Julio D. Aguilar for carrying out the nonlinear dynamic analyses reported in this paper. Similarly, the author gives thanks to Universidad Michoacana de San Nicolás de Hidalgo in Mexico.

References

Applied Technology Council (ATC) (2010) Modeling and acceptance criteria for seismic design and analysis of tall buildings, ATC 72-1, Redwood City, CA, USA

Federal Emergency Management Agency (FEMA) (2012) Seismic performance assessment of buildings. Report FEMA P-58 Vol. 1-Methodology, Washington, DC

Iwata Y, Sugimoto H, Kuguamura H (2006), Reparability limit of steel structural buildings based on the actual data of the Hyogoken-Nanbu earthquake, Proceedings of the 38th Joint Panel. Wind and Seismic effects, NIST Special Publication 1057. pp 23-32

Lignos D and Krawinkler H (2011a), Deterioration modeling of steel components in support of collapse prediction of steel moment frames under earthquake loading, Journal of Structural Engineering, 137(11):1291–1302

Lignos D and Krawinkler H (2011b), Prediction and validation of sidesway collapse of two scale models of a 4-story steel moment frame, Earthquake Engineering and Structural Dynamics, 40:807–825

McCormick J, Aburano H, Ikenaga M, Nakashima M (2008), Permissible residual deformation levels for building structures considering both safety and human elements, Proceedings of the 14th World Conference on Earthquake Engineering, Beijing, China, Paper No. 05-06-0071

OpenSees. Open System for Earthquake Engineering Simulation - Home Page. <http://opensees.berkeley.edu/> (April 1, 2014)

Polese M, Di Ludovico M, Prota A, Manfredi G (2012), Residual capacity of earthquake damaged buildings, 15th World Conference on Earthquake Engineering, Lisbon, Portugal.

Psimoulis P, Stiros S (2007), Measurement of deflections and of oscillation frequencies of engineering structures using robotic theodolites (RTS), Engineering Structures, 29(12): 3312–24

Ruiz-García J and Negrete-Manriquez JC (2011), Evaluation of drift demands in existing steel frames under as-recorded far-field and near-fault mainshock–aftershock seismic sequences, Engineering Structures, 33: 621–634

Zareian F and Medina RA (2009), A practical method for proper modeling of structural damping in inelastic plane structural systems, Computers & Struct, 88: 45-53